ARTICLE

ACS chemical biology

A Fluorescent, Reagentless Biosensor for ADP Based on Tetramethylrhodamine-Labeled ParM

Simone Kunzelmann and Martin R. Webb*

MRC National Institute for Medical Research, The Ridgeway, Mill Hill, London NW7 1AA, United Kingdom

ABSTRACT Fluorescence assays for ADP detection are of considerable current interest, both in basic research and in drug discovery, as they provide a generic method for measuring the activity of ATPases and kinases. The development of a novel fluorescent biosensor is described that is based on a tetramethylrhodamine-labeled, bacterial actin homologue, ParM. The design of the biosensor takes advantage of the large conformational change of ParM on ADP binding and the strong quenching of the tetramethylrhodamine fluorescence by stacking of the dye. ParM was labeled with two tetramethylrhodamines in close proximity, whereby the fluorophores are able to interact with each other. ADP binding alters the distance and relative orientation of the tetramethylrhodamines, which leads to a change in this stacking interaction and so in the fluorescence intensity. The final ADP biosensor shows ~15-fold fluorescence increase in response to ADP binding. It has relatively weak affinity for ADP (K_d = 30 μM), enabling it to be used at substoichiometric concentrations relative to ADP, while reporting ADP concentration changes in a wide range around the K_d value, namely, submicromolar to tens of micromolar. The biosensor strongly discriminates against ATP (>100-fold), allowing ADP detection against a background of millimolar ATP. At 20 °C, the labeled ParM binds ADP with a rate constant of 9.5×10^4 M^{-1} s^{-1} and the complex dissociates at 2.9 s^{-1}. Thus, the biosensor is suitable for real-time measurements, and its performance in such assays is demonstrated using a sugar kinase and a mammalian protein kinase.

ADP is generated in some of the most fundamental biological reactions, catalyzed by two large classes of enzymes, ATPases and kinases. ATP hydrolysis provides the energy for a large number of cellular processes, mediated by ATPases. Kinases are important both in metabolic pathways and in protein phosphorylation, which play a central role in cellular signal transduction. Methods to assay the ADP product are, therefore, of great importance to study these enzymatic reactions, both to understand the enzymes' mechanism of action and to develop inhibitors for therapeutic intervention. Notably, protein kinases are the second most important target for drug screening, following G-protein coupled receptors. ATPases produce free phosphate in addition to ADP, and therefore their activity can be monitored using phosphate detection assays, for example, malachite green (*1*). Kinases transfer the terminal phosphate from ATP onto a substrate, such as a protein, lipid, or sugar, releasing only ADP as a common product of all kinases. Detection of the phosphorylated products requires an assay to be developed for each individual kinase under study. In contrast, ADP-specific sensors provide a generic method to measure the activity of any ATPase or kinase. However, the number of optical assays for ADP detection is still very limited. Examples include coupled enzyme assays (*2*) and recognition by specific RNA molecules (*3*) or by antibodies (*4*–*6*).

Recently we reported a fluorescent, reagentless biosensor for ADP, based on a bacterial actin homologue, ParM, which has a functional role in plasmid segregation *in vivo* (*7*). The rational design of that sensor relied on the large conformational change in ParM that results from ADP binding (*8*). In the nucleotide-free state ParM is in an open conformation, but when ADP binds there is

*Corresponding author, mwebb@nimr.mrc.ac.uk.

Received for review December 21, 2009 and accepted February 16, 2010.

Published online February 16, 2010

10.1021/cb9003173

a large rotation of the two lobes against each other, closing the nucleotide binding cleft. This conformation change was coupled to an optical signal by the attachment of a single coumarin fluorophore, which is sensitive to environmental changes (*7*). Any ADP sensor must discriminate successfully against ATP, which would normally be present in the assay solution, possibly at high concentration. By mutagenesis, ParM was further engineered to achieve strong discrimination against triphosphate binding and to suppress filament formation that occurs in the native protein.

The coumarin-based biosensor MDCC-ParM provides a method for real-time detection of ADP at submicromolar concentrations, such as in transient kinetic experiments. However, due to its low dissociation constant of ADP (0.5 μM), excess MDCC-ParM over ADP is needed when measuring ADP concentrations of >0.5 μM. In addition, the dissociation constant of ATP (~200 μM), albeit much greater than that of ADP, imposes an upper limit on the ATP concentration that can be used.

For several types of assay, criteria such as high sensitivity and fast signal response are not crucial. Such assays would include high-throughput screening and many steady-state measurements. Instead, important criteria may include optical stability, a wide concentration range, in this case of ADP being measured with ATP present, and low reagent usage. Coumarins, as used in the biosensor that was outlined above (*7*), have limited photostability (*9*), and this may be problematic in applications where high-intensity light sources or long illumination periods are used. In addition, assay components may potentially interfere with the optical signal, because the excitation/emission wavelengths of coumarins are relatively low (*10–12*). As mentioned above, relatively high amounts of labeled protein are required, and this may be experimentally inaccessible, for example, due to inner filter effects. Both the target ADP range and reagent usage can be addressed by having a biosensor that reports the ADP concentration without stoichiometric binding and so the concentration of the biosensor can be kept low relative to the ADP being measured. In effect, this issue can be resolved if the biosensor binds ADP weakly.

The development of an ADP biosensor is described here to achieve these aims. The new biosensor is also based on ParM but using a different strategy for signal generation, which relies on formation and dissociation of tetramethylrhodamine stacking. This approach takes advantage of the large difference in rhodamine fluorescence depending on whether the fluorophore is in a monomeric or stacked state. The basis for the fluorescence quenching in the stacked state is exciton coupling (*13–15*). This strategy has been used to monitor cleavage of small peptides by proteases, such as elastase and the malaria protease, PfSUB-1 (*16–18*). When attached to both ends of a peptide, tetramethylrhodamines form the stacking interaction, which largely quenches their fluorescence. This interaction is lost upon cleavage of the peptide yielding an up to 30-fold increase in fluorescence intensity (*14*). The same approach has been used to monitor dissociation of protein complexes and conformation changes in proteins (*19, 20*), where the distance or relative orientation of two attached tetramethylrhodamines alters. An example is a phosphate biosensor that is based on a doubly rhodamine-labeled phosphate binding protein, yielding a 20-fold fluorescence increase upon ligand binding (*19*).

By applying the two-rhodamine strategy to ParM, a new ADP biosensor was developed with characteristics very different from those of MDCC-ParM, previously reported (*7*). The ParM variant, labeled with two tetramethylrhodamines, binds ADP with relatively weak affinity (dissociation constant 30 μM) but responds to ADP binding with ~15-fold signal increase. This means that the tetramethylrhodamine-based biosensor can be used at substoichiometric concentrations, relative to ADP. The sensor strongly discriminates against ATP (K_d >3 mM) and thus enables detection of a wide range of ADP against a background of high ATP concentrations.

RESULTS AND DISCUSSION

Attachment Sites for Double Rhodamine Labeling. In order to label ParM with two tetramethylrhodamines in positions where stacking might occur between them, two accessible cysteine residues were required as specific attachment sites on either side of the nucleotide binding cleft (*8*) (Supplementary Figure 1). The natural exposed cysteine in the wild-type protein was not in a suitable position to provide such a labeling site and was mutated to alanine. Two cysteine mutations were introduced into this ParM mutant (C287A). Two pairs were chosen, D63C/D224C and D63C/K216C, on the basis of the structure (*8*), consideration of distances between labeling sites relative to the structure of the stacked tetramethylrhodamines (*18*), and previous work with tetra-

TABLE 1. Fluorescence changes, nucleotide affinities, and binding dynamics of different tetramethylrhodamine-labeled ParM mutants

	Fluorescence titration[a]					Kinetics[b]		
	ADP		ATP			ADP		
Mutations in addition to D63C, D224C, C287A	(F_+ /F_-)	K_d (μM)	(F_+ /F_-)	K_d (μM)	K_d ratio ATP/ADP	k_{on} (μM^{-1} s^{-1})	k_{off} (s^{-1})	(K_d)[b] (μM)
	5-IATR							
No additional mutation	4.1 ± 0.5	76 ± 3	1.9 ± 0.1	1200 ± 200	16 ± 3	n.d.	n.d.	n.d.
T174A T175N	18.7 ± 0.9	63 ± 3	>6.0	>5000	>80	0.065 ± 0.001	4.2 ± 0.2	65 ± 4
K33A T174A T175N	14.9 ± 0.6	30.2 ± 0.9	>5.0	>3000	>100	0.095 ± 0.007	2.9 ± 0.1	30 ± 4
	6-IATR							
No additional mutation	10 ± 1	147 ± 8	3.7 ± 0.5	1100 ± 100	8 ± 1	n.d.	n.d.	n.d.
T174A T175N	18.9 ± 0.6	103 ± 2	>7.0	>5000	>50	0.055 ± 0.002	6.2 ± 0.2	110 ± 10
K33A T174A T175N	14.5 ± 0.6	37 ± 3	>4.0	>3000	>80	0.074 ± 0.003	3.3 ± 0.3	45 ± 6

[a]Fluorescence titrations were performed as in Figure 1 to determine the equilibrium dissociation constants (K_d) and fluorescence changes (F_+/F_-) upon ADP and ATP binding. Except for the final variant, 5-ATR-ParM (K33A/D63C/T174A/T175N/D224C/C287A), the fluorescence change varied between different batches of labeled protein, since the labeling conditions for the other mutants have not been optimized. Values given in the table represent the maximum fluorescence change observed . [b]Stopped-flow experiments were carried out at 20 °C as described in Figure 3 to determine the association (k_{on}) and dissociation (k_{off}) rate constants for ADP binding. Dissociation constants (K_d) were calculated from k_{off}/k_{on}.

methylrhodamine labeling of phosphate binding protein (*19*). Amino acid positions 224 and 216 are located on helix 8 in subdomain IIB. Position 63 is situated in a loop on the opposing subdomain, which moves away from helix 8 upon ADP binding (Supplementary Figure 1). In the nucleotide-free conformation a tetramethylrhodamine pair attached to these positions should be able to stack, and this interaction may be disrupted when ADP binding induces domain movement.

Test labeling of the two double mutants was done with two rhodamine isomers, 5-IATR and 6-IATR (5- and 6-iodoacetamidotetramethylrhodamine), and the fluorescence response to ADP binding was measured. The labeling stoichiometry was 2:1 as confirmed by mass spectrometry. All four combinations showed an increase in fluorescence on addition of ADP, as expected for the disruption of rhodamine dimers. The larger signal change was observed for ParM (D63C/D224C/C287A) with a 10-fold fluorescence increase when labeled with 6-IATR (Table 1). In contrast, the fluorescence change obtained with ParM (D63C/K216C/C287A) was <3-fold with both tetramethylrhodamine isomers and this could not be improved by further purification of the labeled proteins. Therefore ParM (D63C/D224C/C287A) was chosen for further work.

Optimization of the Biosensor by Mutagenesis. The dissociation constants of ADP binding to 5-IATR- and 6-IATR-labeled ParM (D63C/D224C/C287A) were determined by fluorescence titration to be 76 ± 3 and 147 ± 8 μM, respectively (Figure 1, Table 1). These affinities are orders of magnitude lower than those of wild-type ParM (2.4 μM) (*21*) or the MDCC-labeled ParM version (0.46 μM) (*7*). ATP binds considerably weaker than ADP in both cases, K_d ~1 mM, and the fluorescence change upon triphosphate binding was lower (Figure 1, Table 1). In order to improve ADP selectivity further two active site mutations, T174A and T175N, were introduced into the ParM variant for tetramethylrhodamine labeling. The

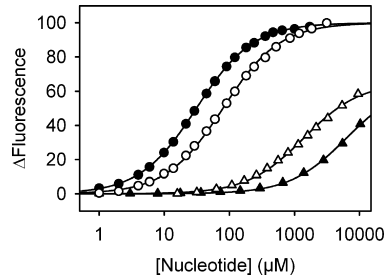

Figure 1. ADP and ATP binding affinity of 5-IATR-labeled ParM. 5-IATR-labeled ParM (D63C/D224C/C287A) (open symbols) and ParM (His_6/K33A/D63C/T174A/T175N/D224C/C287A) (closed symbols), both at a concentration of 0.1 μM, were titrated with ADP (circles) and ATP (triangles). The fluorescence of tetramethylrhodamine was excited at 553 nm and detected at 577 nm. The equilibrium dissociation constants were determined by fitting quadratic binding curves to the data and are listed in Table 1.

same mutations had been successful in decreasing ATP affinity in the MDCC-ParM biosensor (*7*). The new ParM mutant (His_6/D63C/T174A/T175N/D224C/C287A), labeled with either 5-IATR or 6-IATR, had slightly increased ADP affinity, but the mutations weakened ATP binding to >5 mM, thus greatly improving ADP selectivity (Table 1).

Polymerization of 5-IATR- and 6-IATR-labeled ParM (His_6/D63C/T174A/T175N/D224C/C287A) was investigated by right-angle light scattering (data not shown). Both formed filaments in the presence of high ATP concentrations (4 mM), albeit much slower than the wild-type protein (*21, 22*). Therefore an additional mutation (K33A), known to inhibit filament formation (*7, 23*), was introduced into ParM (His_6/D63C/T174A/T175N/D224C/C287A). The new ParM variant, labeled with 5- or 6-IATR, did not show any change in light scattering, even at high ParM concentrations (20 μM) and long incubation times (4 h) (data not shown). Thus the K33A mutation effectively blocks filament formation. The final versions of the ParM (His_6/K33A/D63C/T174A/T175N/D224C/C287A) are hereafter called 5-ATR-(acetamidotetramethylrhodamine)-ParM and 6-ATR-ParM.

Absorbance and Fluorescence Spectra of 5- and 6-ATR-ParM. Fluorescence spectra and absorbance spectra of 5-ATR- and 6-ATR-ParM were measured in the absence and presence of ADP (Figure 2). The absorbance spectrum of 6-ATR-ParM in the absence of ADP is indicative of tetramethylrhodamine stacking with

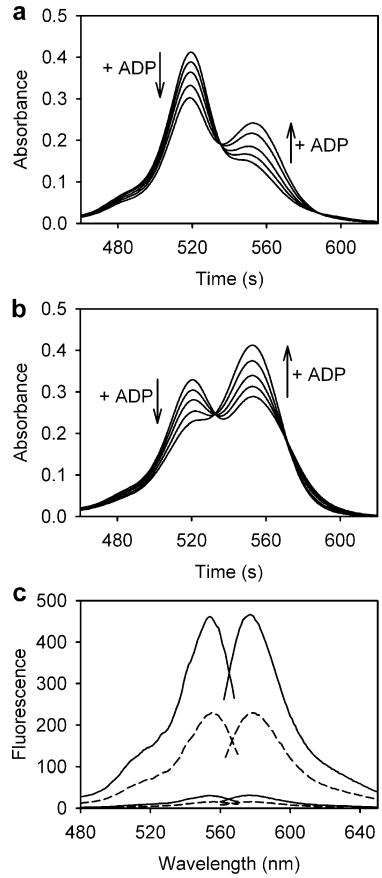

Figure 2. Absorbance and fluorescence spectra of tetramethylrhodamine-labeled ParM. Absorbance spectra of ParM (His_6/K33A/D63C/T174A/T175N/D224C/C287A) labeled with 6-IATR (a) or 5-IATR (b). Spectra were measured in the absence of nucleotide and with 10, 30, 100, and 2000 μM ADP. The spectra show isosbestic points at 535 nm (a) and 532 nm (b). c) Fluorescence excitation and emission spectra of 1 μM 5-IATR-labeled (solid lines) and 6-IATR-labeled (dashed lines) ParM (His_6/K33A/D63C/T174A/T175N/D224C/C287A) in the absence of ADP (lower intensity) and in the presence of 2 mM ADP (higher intensity). Spectra were recorded at 553 and 577 nm excitation and emission wavelengths.

maximum absorbance at 519 nm and a shoulder around 550 nm (Figure 2, panel a). ADP binding causes an absorbance decrease at 519 nm and a concomitant increase in absorbance at 553 nm, indicating that the stacking is disturbed by ADP binding. The absorbance spectra show an isosbestic point at 535 nm. 5-ATR-ParM mutants show different absorbance spectra with a higher absorbance at 553 nm and lower absorbance at

519 nm compared with 6-ATR-ParM (Figure 2, panel b). ADP additions increase the absorbance at 553 nm and decrease the absorbance at 519 nm. The isosbestic point lies at 532 nm. In contrast to the absorbance spectra, the shape of the fluorescence spectra of the two isomers on ParM are almost identical with maximal excitation and emission wavelengths of 553 and 577 nm for 5-ATR-ParM and ~1 nm higher for 6-ATR-ParM (Figure 2, panel c). However, the absolute fluorescence intensity is about 2-fold lower for 6-ATR-ParM.

Both the lower fluorescence obtained with 6-ATR-ParM and the absorbance spectra showing large differences in the intensity ratio of the bands at 519/550 nm indicate that the two rhodamine isomers have a different structural arrangement when attached to the cysteines on ParM. The 6-ATR moieties may form a stronger stacking interaction on ParM, as the absorbance ratio at 519/550 nm is higher and the fluorescence intensity is lower.

ADP and ATP Binding Affinity. The dissociation constants for the final biosensors, 5-ATR- or 6-ATR-ParM, and ADP are 30.2 ± 0.9 and 37 ± 2.5 μM, respectively, as determined by equilibrium titrations (Figure 1 and Table 1). Thus, the K33A mutation increases ADP affinity. In addition, the maximal signal change is slightly lower than for the tetramethylrhodamine-labeled ParM variants without K33A mutation (15-fold instead of 19-fold increase). However, the changes are small and do not seriously affect the biosensor sensitivity.

The dissociation constants of ADP binding to all tetramethylrhodamine-labeled variants are in the range of 30–100 μM, which are much higher values than those of MDCC-ParM (0.5 μM) or wild-type ParM (2.4 μM) (*7, 21*). The strongly reduced nucleotide affinity of IATR-labeled ParM could be due to the larger size of the tetramethylrhodamines, along with the two cysteine mutations affecting the binding. Alternatively the binding of ADP requires the cleft closure and hence the disruption of the rhodamine stacking interaction. A second tetramethylrhodamine-labeled double mutant (D63C/K216C) has more than 10-fold higher ADP affinity than the (D63C/D224C) mutants (data not shown), suggesting that weakened ADP binding is at least in part due to the mutation D224C. In a previous use of tetramethylrhodamine stacking sensing a protein conformation change with the phosphate binding protein, the fluorophores had little effect on the affinity for inorganic phosphate (*19*), suggesting that the stacking *per se* may not necessarily have a significant effect on the energetics. However, in the case of two tetramethylrhodamines attached to a folded protein, their ability to stack and the resulting structure may be much more restricted than in the situation where tetramethylrhodamines are relatively free to find the optimal configuration, either in free solution or attached to a flexible peptide (*18*). Thus the energetics of the stacking may vary between proteins. Indeed, the spectral data with the phosphate binding protein (*19*) suggests such differences do occur. The low affinity makes the tetramethylrhodamine versions less sensitive in comparison to the MDCC sensor but more suitable for high ATP concentrations.

ADP Binding Kinetics. Kinetics of ADP binding to 5-ATR- and 6-ATR-ParM were investigated in stopped-flow experiments taking advantage of the tetramethylrhodamine signal change. Association kinetics were measured under pseudo-first-order conditions with an excess of ADP (Figure 3, panel a). The fluorescence curves were well fit by single exponentials, and the resulting rate constants, k_{obs}, increased with ADP concentration in an approximately linear manner (Figure 3, panel b), indicating that the rate of the signal change is mainly controlled by the bimolecular binding step in the concentration range examined. Data with 6-ATR-ParM show a slight deviation from linearity, indicative of a two-step binding mechanism but too small to deduce kinetic parameters for such a model (Figure 3, inset in panel b and figure legend). Association and dissociation rate constants for a single binding step were calculated from the slope and intercept of linear regression and are summarized in Table 1. The rate constants are similar for the different tetramethylrhodamine-labeled ParM variants. The dissociation constants, obtained from the ratio of rate constants, are in very good agreement with the values determined in equilibrium titrations. Comparison with the ADP binding kinetics of MDCC-ParM (*7*) shows that the strongly reduced ADP affinity in tetramethylrhodamine-labeled ParM (about 2 orders of magnitude) is due to a combination of an order of magnitude reduction in the association rate constant and a similar size increase in the dissociation rate constant. The maximum response time of the tetramethylrhodamine biosensors is defined by the dissociation rate constants, $1/k_{off}$, which is <0.33 s for the slower variant. Thus, the tetramethylrhodamine-based ParM biosensors are well suited for real-time kinetic measurements of ATPase and kinase activity. Finally, the ATP

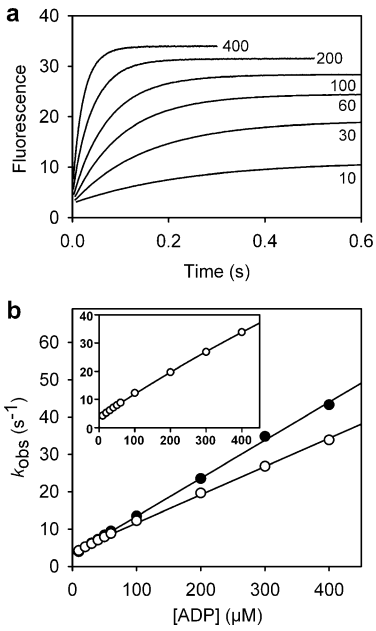

Figure 3. ADP binding kinetics of tetramethylrhodamine-labeled ParM. a) Fluorescence time courses after mixing of 5-ATR-ParM with an excess of ADP in the stopped flow. The concentration of 5-ATR ParM was 0.1 μM (mixing chamber), and the micromolar ADP concentrations after mixing are indicated in the graph. The data shown are averages of three individual stopped-flow traces. The observed rate constants, k_{obs}, were determined by single exponential curve fitting. b) Plot of the observed rate constants versus ADP concentration for 5-ATR- (closed circles) and 6-ATR-ParM (open circles). Association and dissociation rate constants for a one-step binding model, obtained from the slope and intercept of linear regression analysis, are summarized in Table 1. There is a slight deviation from linearity with the 6-ATR-ParM data. One way to explain this is to invoke two-step binding and fit to a hyperbola (inset). However, the accessible concentration range is not large enough to obtain parameters for two steps.

hydrolysis activity of 5-ATR-ParM (His_6/K33A/D63C/T174A/T175N/D224C/C287A) was measured using the phosphate biosensor MDCC-PBP (data not shown) (*24*). The catalytic activity was very low, <0.001 min^{-1}, even at high ParM concentrations (10–20 μM).

As described above, 5-ATR-ParM and 6-ATR-ParM showed rather similar optical and ADP-binding properties. However, the absolute fluorescence of 5-ATR-ParM was ~2-fold greater than that of 6-ATR-ParM (Figure 3, panel c), and this is potentially advantageous in assays using this sensor substoichiometrically. Therefore 5-ATR-ParM was chosen for further study in terms of effect of salt conditions and use in kinase assays.

Effect of Salts on ADP Affinity and Fluorescence Response. All of the measurements described above were performed at one buffer condition, namely, 30 mM Tris·HCl pH 7.5, 25 mM KCl, 3 mM $MgCl_2$. To address the influence of different salt conditions on the biosensor performance, the salt dependencies of nucleotide affinity and fluorescence response were investigated for 5-ATR-ParM (Table 2). Fluorescence titrations were carried out in the presence of different concentrations of potassium and sodium chloride from 0 to 150 mM. 5-ATR-ParM showed the highest ADP affinity in the presence of 150 mM potassium chloride and the lowest affinity in the absence of both salts. The differences in the dissociation constants for ADP are maximum 10-fold between the lowest and highest value. The fluorescence change was less sensitive to the nature and concentration of salt varying between 9- and 15-fold and seemed to correlate with the ADP affinity. Thus, the tetramethylrhodamine biosensors should be applicable to a wide range of salt conditions. However, there is a strict requirement for magnesium ions since the ADP dissociation constant increased to >5 mM, when magnesium ions were removed by EDTA (data not shown).

Kinase Activity Assays Using the ADP Biosensor. As a first example for a kinetic measurement using the tetramethylrhodamine-ParM biosensor, the phosphorylation reaction of D-glucose catalyzed by hexokinase from *Saccharomyces cerevisiae* was examined (Figure 4). Steady-state kinetics of the phosphorylation reaction were measured by monitoring ADP generation with 5-ATR-ParM. The sensor was used at a concentration lower than that of ADP, so that the fractional saturation of tetramethylrhodamine-ParM changes with ADP concentration in a broad range about the dissociation constant. Although at high ADP concentrations this yields a nonlinear relationship between fluorescence signal and ADP, the response was approximately linear at <10 μM ADP (Figure 4, panel a). The presence of 1 mM ATP (the maximum concentration used) increased the background level and so decreased the slope of the calibration curve by about 20% (Figure 4, panel a), and this was accommodated in the calibration as described in Methods. Glucose, at the maximum concentration used in the assay (2 mM), did not significantly alter the sensor response (data not shown). Time courses of ADP generation were monitored either at constant glu-

TABLE 2. Fluorescence changes and dissociation constants of ADP and ATP binding to the final tetramethylrhodamine-ParM biosensor under different salt conditions

	ADP		ATP		
Salt condition	$(F_+/F_-)^a$	K_d (μM)[a]	$(F_+/F_-)^a$	K_d (μM)[a]	K_d ratio ATP/ADP
no additional salt	8.9 ± 0.4	143 ± 1.3	>4	>5000	>35
25 mM KCl	14.9 ± 0.6	30.2 ± 0.9	>6	>3000	>100
150 mM KCl	15.2 ± 0.2	15.3 ± 0.7	>8	>3000	>200
25 mM NaCl	9.4 ± 0.7	86 ± 1.0	>4	>5000	>60
150 mM NaCl	8.8 ± 0.9	114 ± 1.4	>4	>5000	>45
25 mM KCl + 125 mM NaCl	11.2 ± 0.2	88 ± 2.1	>5	>5000	>55

[a]Dissociation constants (K_d) and fluorescence changes upon nucleotide binding (F_+/F_-) to the final biosensor, 5-ATR-ParM (His_6/K33A/D63C/T174A/T175N/D224C/C287A), were determined by fluorescence titrations as described in the legend of Figure 1. Titrations were carried out with 0.5 μM ParM at 20 °C in 30 mM Tris·HCl pH 7.5, 3 mM $MgCl_2$, 5 μM BSA plus the salt indicated.

cose concentration and varying ATP or at constant ATP and increasing glucose concentration. From Michaelis–Menten plots (Figure 4, panels b and c) the parameters $K_M^{ATP} = 75 \pm 2$ μM and $V_{max} = 5.0 \pm 0.2$ μM min^{-1} were obtained for variation of ATP and $K_M^{glucose} = 180 \pm 9$ μM and $V_{max} = 5.4 \pm 0.2$ μM min^{-1} for variation of the D-glucose concentration. The V_{max} values yield an average activity of 1.04 ± 0.05 μmol min^{-1} per unit of hexokinase, which is in good agreement with the unit definition of the supplier, 1 μM min^{-1} $unit^{-1}$, under similar experimental conditions (pH 7.6, 25 °C).

A second example of a kinase assay was performed with mammalian, AMP-activated protein kinase, a key enzyme in sensing cellular energy levels and controlling metabolism in response to nutrients and hormones (*25*). Phosphorylation kinetics of SAMS peptide, a peptide derived from acetyl-CoA carboxylase with a single phosphorylation site (*26*), was measured using 5-ATR-ParM (Figure 5). In two sets of kinetic experiments, either varying ATP or the concentration of SAMS peptide, the time courses of ADP generation were monitored and the initial rates were determined (Figure 5, insets). Michaelis–Menten plots of the results from the two data sets are shown in Figure 5, panel a and b. The Michaelis–Menten parameters $K_M^{ATP} = 35 \pm 3$ μM and $V_{max} = 20 \pm 2$ nM s^{-1} were obtained from variation of ATP and $K_M^{SAMS} = 36 \pm 1$ μM and $V_{max} = 19 \pm 1$ nM s^{-1} from data at different SAMS concentration. The average value for the catalytic constant is $k_{cat} = 9.8 \pm 0.6$ s^{-1}. The K_M value for SAMS peptide is in good agreement with data from other groups using either the recombinant, phosphorylated enzyme ($K_M = 47$ μM (*27*)) or the native rat liver enzyme ($K_M = 30$ μM (*26*)). The K_M value for ATP is about 2-fold lower than the 86 μM measured previously (*28*) using acetyl-CoA carboxylase as substrate.

Performance of the Final ADP Biosensor. From the four different ParM variants, doubly labeled with tetramethylrhodamine, 5-ATR-ParM (His_6/K33A/D63C/T174A/T175N/D224C/C287A) is likely to be generally the most suitable ADP biosensor. Although the labeling with the two isomers, 5- and 6-IATR, gives similar ADP binding properties and signal change, the absolute fluorescence levels are higher with 5-ATR-ParM.

The tetramethylrhodamine-labeled ParM has some characteristics very different from those of the coumarin-labeled version (*7*) and so different potential applications as a biosensor for ADP. The first important difference is that the 5-ATR-ParM can be used at lower concentration than the ADP to be detected. Because of the weak binding, the degree of saturation and thus the fluorescence will vary with ADP in a wide range around the dissociation constant. While this method of measurement is inherently less sensitive than quantitative capture of ADP by a high affinity sensor, it has the large advantage of requiring only low concentration of the biosensor in the assay solution. A high concentration of protein may interfere negatively with the assay, for example, interacting with some component or introducing inner filter effects, but is also expensive in material. In

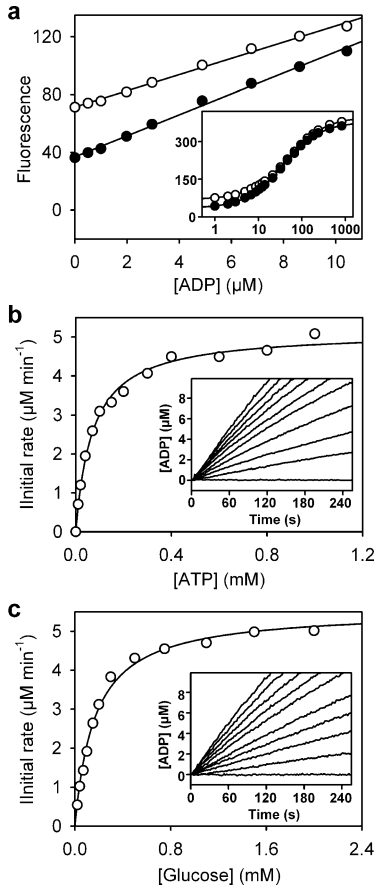

Figure 4. Steady-state assay of hexokinase activity using the ADP biosensor. Phosphorylation of D-(+)-glucose by hexokinase (0.005 units mL^{-1}) was measured by monitoring ADP generation with 5-ATR-ParM (0.25 μM). a) Calibration of the fluorescence signal; 0.25 μM 5-ATR-ParM was titrated with ADP in the absence (closed circles) and in the presence of 1 mM ATP (open circles). The slopes of linear regression analysis of data with 0 and 1 mM ATP are 6.8 ± 0.2 and 5.4 ± 0.1 μM^{-1}, respectively. The inset shows the complete titration curves on a logarithmic scale. The axis descriptions are the same as in the main graph. b) Phosphorylation kinetics at varying ATP concentration and constant 2 mM glucose. Initial rates are plotted versus ATP concentration. Curve fitting according to the Michaelis–Menten equation results in the parameters K_M = 75 ± 2 μM and V_{max} = 5.0 ± 0.2 μM min^{-1}. The inset shows the time courses of ADP generation at 0, 0.01, 0.02, 0.04, 0.07, 0.1, 0.2, 0.3, 0.6, and 1 mM ATP. c) Plot of the initial rates versus glucose concentration, measured at 1 mM ATP. The Michaelis–Menten parameters of the fitted curve are K_M, 180 ± 9 μM, and V_{max}, 5.4 ± 0.2 μM min^{-1}. The inset shows the time courses of ADP generation at 0, 0.02, 0.04, 0.07, 0.1, 0.15, 0.2, 0.3, 0.5, and 2 mM glucose.

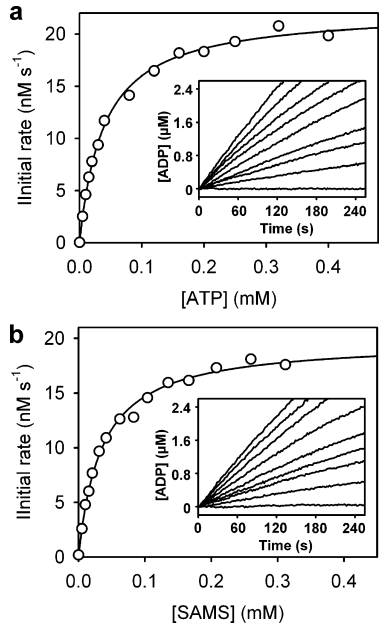

Figure 5. Steady-state assay of AMP kinase activity using the ADP biosensor. Kinetics of phosphorylation of SAMS peptide by AMP kinase (2 nM) was measured by monitoring ADP generation using 5-ATR-ParM (0.5 μM). a) Plot of the initial rates versus ATP concentration measured at constant 300 μM SAMS peptide. Curve fitting according to the Michaelis–Menten equation results in the parameters K_M = 35 ± 3 μM, and V_{max}, 20 ± 2 nM s^{-1}. Inset: Time courses of ADP generation at 0, 5, 10, 15, 30, 40, 80, 120, and 400 μM ATP. b) Plot of the initial rates versus SAMS peptide concentration. The data were obtained at constant 400 μM ATP. The Michaelis–Menten parameters from the fitted curve are K_M = 36 ± 1 μM, and V_{max}, 19 ± 1 nM s^{-1}. Inset: Time courses of ADP generation at 0, 5, 10, 15, 20, 40, 60, 100, 160, and 300 μM SAMS peptide.

practice, the required concentration of sensor protein would be determined mainly by the sensitivity of the optical detection system, the absolute fluorescence of the sensor itself, and the accuracy required. As shown in the kinase assays, submicromolar concentrations of the sensor can be easily used. Another practical consequence of the weak nucleotide binding is that ADP contamination in ATP would be less problematic than with MDCC-ParM.

A second important advantage is the very weak ATP binding of the tetramethylrhodamine-labeled sensor, which allows use of high ATP concentrations. This is important, for example, where a very broad concentration range is required for systems with different K_M values. As

the kinase assays (Figure 4 and Figure 5) demonstrate, low micromolar to submicromolar ADP concentrations can be detected on the background of millimolar ATP. Finally, tetramethylrhodamine is generally more photostable than coumarins (*9*), and the fluorescence is excited and detected at higher wavelengths. These properties are likely to make tetramethylrhodamine-ParM more suitable for applications that require high intensity and/or long illumination and where optical interference with other assay components is critical, such as in high-throughput screening. The low nucleotide affinity and optical properties of ATR-ParM are also a good starting point for further development of the biosensor to enable ADP measurement in cells.

METHODS

Plasmids. ParM expression plasmids were derived from plasmid pJSC1 (*7, 23*). Point mutations in ParM were introduced by QuikChange site-directed mutagenesis (Stratagene). All ParM variants except the triple mutants ParM (D63C/D224C/C287A) and (D63C/K216C/C287A) contain a hexahistidine tag at the C-terminus, generated by site-directed mutagenesis as described previously (*7*).

Expression and Purification of ParM Mutants. ParM variants were synthesized in *E. coli* BL21-Ai cells (Invitrogen) as described (*7*). ParM without an affinity tag was purified by polymerization/depolymerization, His_6-tagged ParM was purified by Ni-chelate affinity chromatography (HisTrap HP, GE Healthcare), both followed by size exclusion chromatography on Superdex 75 (GE Healthcare). The purification was performed as described in detail previously (*7*) with the following modifications. The buffers for Ni-chelate chromatography were supplemented with 1 mM tris(2-carboxyethyl)phosphine, and the buffer for size exclusion chromatography was supplemented with 5 mM DTT. Concentration of ParM mutants was determined by absorbance measurements using the extinction coefficient 34,380 M^{-1} cm^{-1} at 280 nm, calculated from the primary sequence (*29*).

Labeling of ParM Mutants with IATR. All steps were performed in 30 mM Tris·HCl pH 7.5, 25 mM KCl. Before labeling, DTT was removed on a PD10 column (GE Healthcare). Double labeling with tetramethylrhodamine was typically performed on a scale of 10–20 mg protein. One hundred micromolar ParM and 400 μM 5- or 6-IATR (*30, 31*) were incubated in degassed buffer at 22 °C with end-over-end stirring for 90 min. Next, 2 mM sodium 2-mercaptoethanesulfonate was added, and stirring was continued for another 15 min. Reaction mixtures were centrifuged (14,000*g*, 10 min, 4 °C), and the supernatant was filtered through a 0.2 μm syringe filter (Acrodisc, Pall Corporation). Excess fluorophore and sodium 2-mercaptoethanesulfonate were removed on a PD10 column (GE Healthcare). The eluate was loaded on a 1 mL HiTrapQ HP column (GE Healthcare). The column was washed (10 column volumes), and the labeled ParM was eluted by applying a linear gradient of 25–200 mM KCl over 40 column volumes. Fractions showing the highest fluorescence change upon ADP binding were pooled, and the labeled protein was concentrated in an Amicon Ultracentrifugal filter device (Millipore Corporation) to ~10 mg mL^{-1}. Aliquots were shock-frozen in liquid nitrogen and stored at −80 °C. Double labeling was confirmed by electrospray-ionization mass spectrometry. The measured masses differed by <0.5 Da from the theoretical values for the doubly labeled proteins. Concentration of tetramethylrhodamine-labeled ParM mutants were determined from the absorbance spectra using the extinction coefficient of a small molecule thiol adduct of 5-IATR at its isosbestic point, ε_{528} = 52,000 M^{-1} cm^{-1} (*31*). Note that differences in the spectra when attached to ParM may lead to a small error in the calculated concentrations.

Nucleotides. ADP and ATP (Sigma-Aldrich) were purchased at the highest purity available. ATP was further purified by anion-exchange, and the purity of nucleotides was analyzed by HPLC as described (*7*). The concentrations of ADP and ATP were determined from their absorbance spectra in 20 mM Tris·HCl pH 7.5 using the extinction coefficient ε_{259} = 15,400 cm^{-1}.

Fluorescence and Light Scattering Measurements. Fluorescence spectra and titrations were measured in a Cary Eclipse spectrofluorimeter (Varian). Excitation and emission spectra were recorded with 5 nm slit width at emission and excitation wavelength of 577 and 553 nm, respectively. In titration experiments tetramethylrhodamine fluorescence was measured at the same excitation/emission wavelength. Titration data were analyzed with a quadratic binding curve using the program Grafit 5.0 (*7*).

Stopped-flow experiments were performed using a HiTech SF61 DX2 instrument equipped with a Xe/Hg lamp (TgK Scientific). Association kinetics of tetramethylrhodamine-labeled ParM and ADP was measured under pseudo-first-order conditions by mixing 0.2 μM labeled ParM (syringe concentration) with excess ADP. Tetramethylrhodamine fluorescence was excited at 553 nm and fluorescence emission was detected after passing 570 nm cutoff filter. Data were analyzed by single exponential curve fitting using KinetAsyst 3 (TgK Scientific) All fluorescence measurements were carried out in 30 mM Tris·HCl pH 7.5, 25 mM KCl, 3 mM $MgCl_2$, and 5 μM BSA at 20 °C unless stated otherwise.

Filament formation of labeled ParM mutants was measured by right angle light scattering at 340 nm in a Cary Eclipse spectrofluorimeter (Varian) as described (*7*). The assay was performed at 20 °C in 30 mM Tris·HCl pH 7.5, 25 mM KCl, 3 mM $MgCl_2$.

Steady-State Assays of Hexokinase and AMP Kinase Activity. Kinetics of phosphorylation of D-(+)-glucose by hexokinase from *S. cerevisiae* (Sigma-Aldrich) were monitored with the ADP biosensor 5-ATR-ParM (His_6/K33A/D63C/T174A/T175N/D224C/C287A) using a Cary Eclipse spectrofluorimeter (Varian). Measurements were carried out in 50 mM Tris·HCl pH 7.5, 25 mM KCl, 10 mM $MgCl_2$, and 2.5 μM BSA at 20 °C. Reactions were set up with 0.25 μM 5-ATR-ParM, 0.005 unit mL^{-1} hexokinase, and at constant 1 mM ATP and varying concentrations of glucose (20–2000 μM) or at constant 2 mM glucose and increasing ATP concentrations. The reaction was started by the addition of hexokinase. Tetramethylrhodamine fluorescence was excited at 553 nm and detected at 577 nm. For calibration of the fluorescence signal 0.25 μM 5-ATR-ParM was titrated with ADP in the absence of ATP and in the presence of 1 mM ATP (maximal concentration used). In the range up to ~10 μM ADP the data could be approximated by a linear dependence (Figure 4, panel a). The slope from linear regression analysis was 6.8 ± 0.2 μM^{-1} in the absence of ATP and about 20% lower, 5.4 ± 0.1 μM^{-1}, in the presence of 1 mM ATP (Figure 4, panel a). The latter value was used to calibrate all data obtained at maximum ATP (1 mM).

For calibration of the measurements at lower ATP concentrations, a slope for calibration was calculated by linear interpolation between the values at 0 and 1 mM ATP. In contrast to ATP, glucose (2 mM) did not have a significant effect on the fluorescence response of tetramethylrhodamine-ParM.

Phosphorylation kinetics of SAMS peptide (*26*) by AMP kinase (phosphorylated, heterotrimeric complex, $\alpha\beta\gamma$) (*27*) were measured using 5-ATR-ParM (His_6/K33A/D63C/T174A/T175N/D224C/C287A) analogous to the procedure described for the hexokinase assay. Measurements were carried out in 50 mM Tris·HCl pH 7.5, 80 mM KCl, 5 mM $MgCl_2$, 2 mM DTT, and 5 μM BSA at 20 °C. The concentrations used were 2 nM AMP kinase, 0.5 μM ParM and either constant 400 μM ATP and varying concentrations of SAMS peptide or constant 300 μM SAMS peptide and varying ATP.

All experiments were performed at least in duplicate and values given in the text, tables, and figure legends are averages of these.

Acknowledgment: This work was supported by Medical Research Council Technology and by the Medical Research Council, U.K. We thank J. Salje and J. Löwe (MRC Laboratory of Molecular Biology, Cambridge, UK) for providing the plasmid pJSC1 for ParM expression. We thank S. Howell (NIMR, London, UK) for recording the mass spectra, B. Xiao and R. Heath (NIMR, London, UK) for the gift of purified and phosphorylated AMP kinase, J. Corrie (NIMR, London, UK) for the gift of 6-IATR and 5-IATR, G. Reid (NIMR, London, UK) for purification of the ATP, and K. Ansell (MRC Technology) for helpful discussions.

Supporting Information Available: This material is available free of charge *via* the Internet at http://pubs.acs.org.

REFERENCES

1. Itaya, K., and Ui, M. (1966) A new micromethod for the colorimetric determination of inorganic phosphate, *Clin. Chim. Acta 14*, 361–366.
2. Charter, N. W., Kauffman, L., Singh, R., and Eglen, R. M. (2006) A generic, homogenous method for measuring kinase and inhibitor activity via adenosine 5′-diphosphate accumulation, *J. Biomol. Screen. 11*, 390–399.
3. Srinivasan, J., Cload, S. T., Hamaguchi, N., Kurz, J., Keene, S., Kurz, M., Boomer, R. M., Blanchard, J., Epstein, D., Wilson, C., and Diener, J. L. (2004) ADP-specific sensors enable universal assay of protein kinase activity, *Chem. Biol. 11*, 499–508.
4. Kleman-Leyer, K. M., Klink, T. A., Kopp, A. L., Westermeyer, T. A., Koeff, M. D., Larson, B. R., Worzella, T. J., Pinchard, C. A., van de Kar, S. A., Zaman, G. J., Homberg, J. J., and Lowery, R. G. (2009) Characterization and optimization of a red-shifted fluorescence polarization ADP detection assay, *Assay Drug Dev. Technol. 7*, 56–67.
5. Hong, L., Quinn, C. M., and Jia, Y. (2009) Evaluating the utility of the HTRF® Transcreener(TM) ADP assay technology: a comparison with the standard HTRF assay technology, *Anal. Biochem. 391*, 31–38.
6. Lowery, R. G., and Kleman-Leyer, K. (2006) Transcreener: screening enzymes involved in covalent regulation, *Expert Opin. Ther. Targets 10*, 179–190.
7. Kunzelmann, S., and Webb, M. R. (2009) A biosensor for fluorescent determination of ADP with high time resolution, *J. Biol. Chem. 284*, 33130–33138.
8. van den Ent, F., Moller-Jensen, J., Amos, L. A., Gerdes, K., and Lowe, J. (2002) F-actin-like filaments formed by plasmid segregation protein ParM, *EMBO J. 21*, 6935–6943.
9. Eggeling, C., Widengren, J., Rigler, R., and Seidel, C. A. M. (1998) Photobleaching of fluorescent dyes under conditions used for single-molecule detection: evidence of two-step photolysis, *Anal. Chem. 70*, 2651–2659.
10. Simeonov, A., Jadhav, A., Thomas, C. J., Wang, Y., Huang, R., Southall, N. T., Shinn, P., Smith, J., Austin, C. P., Auld, D. S., and Inglese, J. (2008) Fluorescence spectroscopic profiling of compound libraries, *J. Med. Chem. 51*, 2363–2371.
11. Grant, S. K., Sklar, J. G., and Cummings, R. T. (2002) Development of novel assays for proteolytic enzymes using rhodamine-based fluorogenic substrates, *J. Biomol. Screen. 7*, 531–540.
12. Turek-Etienne, T. C., Small, E. C., Soh, S. C., Xin, T. A., Gaitonde, P. V., Barrabee, E. B., Hart, R. F., and Bryant, R. W. (2003) Evaluation of fluorescent compound interference in 4 fluorescence polarization assays: 2 kinases, 1 protease, and 1 phosphatase, *J. Biomol. Screen. 8*, 176–184.
13. Kasha, M. (1963) Energy transfer mechanisms and the molecular exciton model for molecular aggregates, *Radiat. Res. 20*, 55–70.
14. Kasha, M., Rawls, H. R., and Ashraf El-Bayoumi, M. (1965) The exciton model in molecular spectroscopy, *Pure Appl. Chem. 11*, 371–392.
15. Scholes, G. D., and Ghiggino, K. P. (1994) Electronic interactions and interchromophore electron transfer, *J. Phys. Chem. 98*, 4580–4590.
16. Packard, B. Z., Toptygin, D. D., Komoriya, A., and Brand, L. (1996) Profluorescent protease substrates: intramolecular dimers described by the exciton model, *Proc. Natl. Acad. Sci. U.S.A. 93*, 11640–11645.
17. Packard, B. Z., Toptygin, D. D., Komoriya, A., and Brand, L. (1997) Design of profluorescent protease substrates guided by exciton theory, *Methods Enzymol. 278*, 15–23.
18. Blackman, M. J., Corrie, J. E. T., Croney, J. C., Kelly, G., Eccleston, J. F., and Jameson, D. M. (2002) Structural and biochemical characterization of a fluorogenic rhodamine-labeled malarial protease substrate, *Biochemistry 41*, 12244–12252.
19. Okoh, M. P., Hunter, J. L., Corrie, J. E. T., and Webb, M. R. (2006) A biosensor for inorganic phosphate using a rhodamine-labeled phosphate binding protein, *Biochemistry 45*, 14764–14771.
20. Hamman, B. D., Oleinikov, A. V., Jokhadze, G. G., Bochkariov, D. E., Traut, R. R., and Jameson, D. M. (1996) Tetramethylrhodamine dimer formation as a spectroscopic probe of the conformation of *Escherichia coli* ribosomal protein L7/L12 dimers, *J. Biol. Chem. 271*, 7568–7573.
21. Garner, E. C., Campbell, C. S., and Mullins, R. D. (2004) Dynamic instability in a DNA-segregating prokaryotic actin homolog, *Science 306*, 1021–1025.
22. Popp, D., Yamamoto, A., Iwasa, M., Narita, A., Maeda, K., and Maeda, Y. (2007) Concerning the dynamic instability of actin homolog ParM, *Biochem. Biophys. Res. Commun. 353*, 109–114.
23. Salje, J., and Lowe, J. (2008) Bacterial actin: architecture of the ParMRC plasmid DNA partitioning complex, *EMBO J. 27*, 2230–2238.
24. Brune, M., Hunter, J. L., Howell, S. A., Martin, S. R., Hazlett, T. L., Corrie, J. E. T., and Webb, M. R. (1998) Mechanism of inorganic phosphate interaction with phosphate binding protein from *Escherichia coli*, *Biochemistry 37*, 10370–10380.
25. Kahn, B. B., Alquier, T., Carling, D., and Hardie, D. G. (2005) AMP-activated protein kinase: ancient energy gauge provides clues to modern understanding of metabolism, *Cell Metab. 1*, 15–25.
26. Davies, S. P., Carling, D., and Hardie, D. G. (1989) Tissue distribution of the AMP-activated protein kinase, and lack of activation by cyclic-AMP-dependent protein kinase, studied using a specific and sensitive peptide assay, *Eur. J. Biochem. 186*, 123–128.
27. Neumann, D., Woods, A., Carling, D., Wallimann, T., and Schlattner, U. (2003) Mammalian AMP-activated protein kinase: functional, heterotrimeric complexes by co-expression of subunits in *Escherichia coli*, *Protein Expression Purif. 30*, 230–237.
28. Carling, D., Clarke, P. R., Zammit, V. A., and Hardie, D. G. (1989) Purification and characterization of the AMP-activated protein kinase, *Eur. J. Biochem. 186*, 129–136.

29. Pace, C. N., Vajdos, F., Fee, L., Grimsley, G., and Gray, T. (1995) How to measure and predict the molar absorption coefficient of a protein, *Protein Sci. 4*, 2411–2423.
30. Munasinghe, V. R. N., and Corrie, J. E. T. (2006) Optimised synthesis of 6-iodoacetamidotetramethylrhodamine, *ARKIVOC ii*, 143–149.
31. Corrie, J. E. T., and Craik, J. S. (1994) Synthesis and characterisation of pure isomers of iodoacetamidotetramethylrhodamine, *J. Chem. Soc., Perkin Trans. 1* 2967–2973.